Chapter 34

Nested gamma-theta rhythms

In many brain structures, in particular in the hippocampus, gamma oscillations appear near the crests of much slower, 4–11 Hz oscillations, called *theta oscillations* or *theta rhythms*. For an example, see Fig. 34.1.

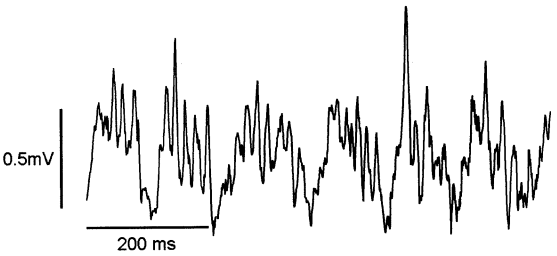

Figure 34.1. *Figure 4A of [23], showing gamma oscillations riding (primarily) on the crests of theta oscillations in an* in vivo *local field potential recording from the CA1 region of mouse hippocampus. Reproduced with publisher's permission.*

In rodents, theta oscillations have been linked to exploratory behavior [22], and to learning and memory [71]. Furthermore, gamma oscillations nested in theta oscillations have been hypothesized to serve the purpose of "representing multiple items in an ordered way" [105], with different gamma sub-cycles of the theta cycle corresponding to different items. Note that the number of gamma cycles that fit into a theta cycle is about seven: 20 ms and 140 ms are typical durations of gamma and theta cycles, respectively. Lisman and Idiart [104] have suggested that this may be the reason why the maximal number of items that humans can typically hold in brief, transient memory (*working memory*) is on the order of seven (plus or minus two) [117]. Most of us can briefly hold a seven-digit phone number in memory, while

we are looking for the phone, but few of us could do the same with a fourteen-digit phone number.

Computationally, one can obtain a gamma oscillation riding on the crests of a theta oscillation simply by driving the E-cells in a PING network at theta frequency; see Section 34.1. Qualitatively, this might model a theta rhythm that is "externally imposed", projected into the network that we are studying from another brain structure, somewhat reminiscent of a suggestion in [24] that inhibitory "supernetworks" rhythmically entrain large populations of pyramidal cells throughout the brain.

A model network that *intrinsically* generates both the theta rhythm and the gamma rhythm nested in it can be obtained by adding to a PING network a second class of inhibitory cells intrinsically firing at theta frequency. We will call this new class of inhibitory cells the *O-cells*, a terminology that will be motivated shortly. If the O-cells received no input from the PING network, and if they synchronized, then this would not be very different from the PING networks driven at theta frequency discussed in Section 34.1. However, a mechanism by which the O-cells can synchronize is needed. One natural such mechanism would be common input from the PING network. For nested gamma-theta oscillations to result, the O-cells must allow several gamma cycles between any two of their population spike volleys. This can be accomplished in a robust way if the O-cells express a slowly building depolarizing current that is rapidly reduced by firing, such as an h-current, or a slowly decaying hyperpolarizing current that is rapidly raised by firing, such as a firing-induced slow potassium current. Several model networks generating nested gamma-theta rhythms following these ideas have been proposed; examples can be found in [155] and [171].

In Sections 34.2 and 34.3, we describe (in essence) the model from [155], in which the second class of inhibitory cells represent the so-called *oriens lacunosum-moleculare (O-LM) interneurons* [89] of the hippocampus; this is the reason for the name *O-cells*.

34.1 Gamma rhythms riding on externally imposed theta rhythms

Figures 34.2 and 34.3 show examples of PING networks with external input to the E-cells oscillating at theta frequency (8 Hz). In Fig. 34.2, the oscillatory input is a sinusoidal injected *current*, whereas in Fig. 34.3, it is (a bit more in line with [24]) *synaptic* inhibition with an oscillating synaptic gating variable. In both figures, we see bursts of gamma frequency oscillations, occurring in theta frequency packets.

Note that the local field potential in Fig. 34.1 looks quite different from the mean membrane potentials of the E-cells depicted in the middle panels of Figs. 34.2 and 34.3, and from the mean E-cell gating variables depicted in the lower panels of Figs. 34.2 and 34.3. However, this by itself does not necessarily imply that the nested gamma-theta rhythm of Fig. 34.1 has to be fundamentally different from a PING network driven at theta frequency; we don't know what is a good analogue of the LFP in our model networks, and neither the mean membrane potential of the

E-cells, nor the mean gating variable of the E-cells, are likely to be good analogues.

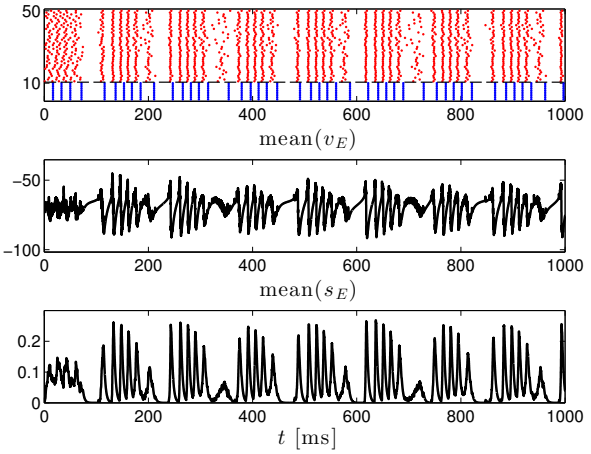

Figure 34.2. *A PING network with external drive to the E-cells oscillating at theta frequency. Spike rastergram (top panel), mean of membrane potentials of E-cells (middle panel), mean of gating variables of E-cells (bottom panel). The parameters of the PING network are* $N_E = 40$, $N_I = 10$, $\overline{I}_E = 1.4$, $\sigma_E = 0.05$, $\overline{I}_I = 0$, $\hat{g}_{EE} = 0$, $\hat{g}_{EI} = 0.25$, $\hat{g}_{IE} = 0.25$, $\hat{g}_{II} = 0.25$, $p_{EI} = 1$, $p_{IE} = 1$, $p_{II} = 1$, $\tau_{r,E} = 0.5$, $\tau_{\text{peak},E} = 0.5$, $\tau_{d,E} = 3$, $v_{\text{rev},E} = 0$, $\tau_{r,I} = 0.5$, $\tau_{\text{peak},I} = 0.5$, $\tau_{d,I} = 9$, $v_{\text{rev},I} = -75$. *The actual drive to the i-th E-cell, however, is not* $I_{E,i} = \overline{I}_E(1 + \sigma_E X_i)$, *but* $(1 + 0.8\sin(2\pi t/125))\, I_{E,i}$, *i.e., it oscillates with period 125 ms, or frequency 8 Hz.* [PING_WITH_THETA_DRIVE]

34.2 A model O-LM celll

The cell bodies of the hippocampal *oriens lacunosum-moleculare (O-LM) interneurons* [89] lie in a deep layer of the hippocampus called the *stratum oriens*. Their axonal arbors lie in a superficial layer called the *stratum lacunosum-moleculare*. This explains their name.

O-LM cells are *somatostatin-positive* (SOM+), i.e., they contain the hormone somatostatin. They inhibit *distal dendrites* (dendrites far from the cell body) of pyramidal cells. This is in contrast with the fast-firing basket cells instrumental in generating gamma oscillations, which are *parvalbumin-positive* (PV+) and inhibit pyramidal cells *perisomatically*, i.e., near the cell body. Since we use single-compartment model neurons, the difference between inhibition of distal dendrites and perisomatic inhibition is not represented in our models. However, following [155], we will assume that the inhibitory input to pyramidal cells from O-LM cells rises and decays more *slowly* than that from fast-firing basket cells. This assumption is in line with experimental evidence; see [69].

In Section 34.3, the O-LM cells will play the role of pacing the theta oscillation.

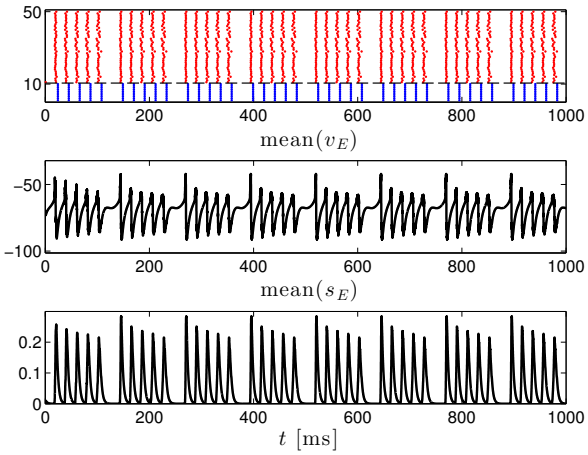

Figure 34.3. *Same as Fig. 34.2, but the external current inputs are constant in time ($I_{E,i} = \overline{I}_E(1 + \sigma_E X_i)$), and instead the pulsatile synaptic input $0.2e^{-10\sin^2(\pi t/125)}(v_{\mathrm{rev},I} - v)$ is added to each E-cell.* [PING_WITH_THETA_INHIBITION]

As discussed in the introduction to this chapter, for them to be able to do that robustly, they should express a slowly building depolarizing current that is rapidly reduced by firing, or a slowly decaying hyperpolarizing current that is rapidly raised by firing. In the model of [155], they are assumed to express an h-current, which is rapidly reduced by firing and slowly builds up between action potentials; this is in agreement with experimental evidence [108]. The model O-LM cells of [155] also express a transient (inactivating) hyperpolarizing potassium current called an *A-current*, again in agreement with experimental evidence [187]. This current will be discussed in detail later.

In [155], the h- and A-currents were added to a single-compartment model with the standard Hodgkin-Huxley currents, that is, the spike-generating sodium, delayed rectifier potassium, and leak currents. That model was of the same form as the RTM and WB models from Sections 5.1 and 5.2, except for the assumption $m = m_\infty(v)$, which was made in Sections 5.1 and 5.2, but not in [155]. We modify the model of [155] in that regard, i.e., we do set $m = m_\infty(v)$. Thus the form of our O-LM cell model, without the h- and A-currents, is precisely the same as that of the RTM and WB models. The constants are

$$C = 1.3\,\mu\mathrm{F/cm}^2, \quad v_{\mathrm{Na}} = 90\,\mathrm{mV}, \quad v_{\mathrm{K}} = -100\,\mathrm{mV}, \quad v_{\mathrm{L}} = -70\,\mathrm{mV},$$
$$\overline{g}_{\mathrm{Na}} = 30\,\mathrm{mS/cm}^2, \quad \overline{g}_{\mathrm{K}} = 23\,\mathrm{mS/cm}^2, \quad \overline{g}_{\mathrm{L}} = 0.05\,\mathrm{mS/cm}^2.$$

The functions α_x and β_x, $x = m, h, n$, are

$$\alpha_m(v) = \frac{0.1(v+38)}{1-\exp(-(v+38)/10))}, \qquad \beta_m(v) = 4\exp(-(v+65)/18),$$
$$\alpha_h(v) = 0.07\exp(-(v+63)/20), \qquad \beta_h(v) = \frac{1}{1+\exp(-(v+33)/10)},$$

$$\alpha_n(v) = \frac{0.018(v-25)}{1-\exp(-(v-25)/25)}, \qquad \beta_n(v) = \frac{0.0036(35-v)}{1-\exp(-(35-v)/12)}.$$

Figure 34.4 shows the graphs of x_∞ and τ_x, $x = m$, h, and n. A comparison with the blue, dash-dotted curves in Fig. 5.1 shows that the most striking difference between this model and the WB model is that the inactivation variable, h, of the spike-generating sodium current is much slower here. This results in fairly broad action potentials; see Fig. 34.5, and compare with Fig. 5.3.

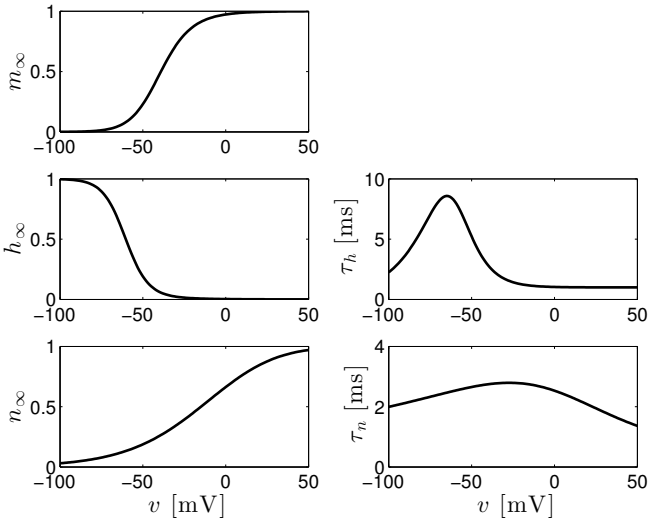

Figure 34.4. *The functions x_∞ and τ_x in the O-LM cell model of [155], but without the h- and A-currents. We left out τ_m because we set $m = m_\infty(v)$.* [PRE_OLM_X_INF_TAU_X]

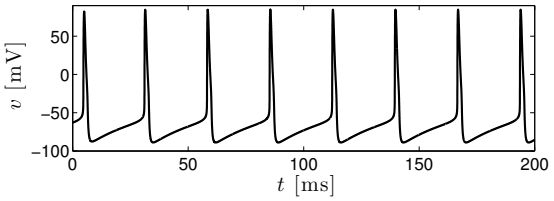

Figure 34.5. *Voltage trace of the O-LM cell model of [155], but without the h- and A-currents, and with $m = m_\infty(v)$. In this simulation, $I = 1.5\,\mu A/cm^2$.* [PRE_OLM_VOLTAGE_TRACE]

We now add the h-current defined by eqs. (18.1)–(18.3) to this model. Following [155], we use $\overline{g}_{\rm h} = 12\,{\rm mS/cm^2}$. The resulting voltage trace is shown in Fig. 34.6, upper panel. The graph of r (lower panel of Fig. 34.6) shows that indeed the h-current plummets to near zero in response to an action potential, then rises more

gradually. Note that addition of the h-current significantly accelerates the neuron: Compare Fig. 34.5 with Fig. 34.6. The reason is that $v_{\rm h} = -32.9\,{\rm mV}$ is far above rest.

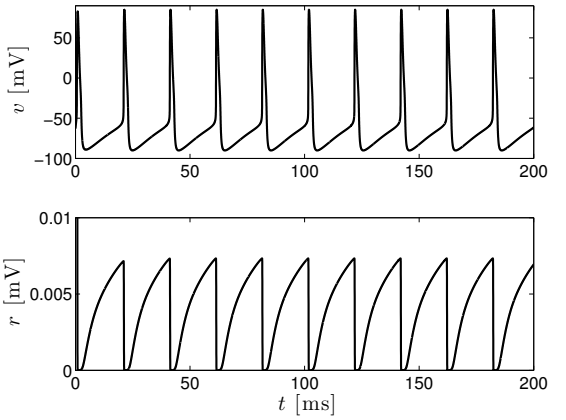

Figure 34.6. *Upper panel: Same as Fig. 34.5, but with h-current defined by eqs. (18.1)–(18.3), with* $\overline{g}_{\rm h} = 12\,mS/cm^2$*, and with* $I = 0\,\mu A/cm^2$*. Lower panel: Gating variable,* r*, of the h-current (see eqs. (18.1)–(18.3)).* [OLM_WITH_H_CURRENT]

Finally, we consider the model *A-current* of [155]. An A-current is a slowly decaying hyperpolarizing potassium current, rapidly raised by firing. This description makes it sound very similar to adaptation of the kind we discussed in Chapter 9. What is special about the A-current, however, is that it is *transient*, i.e., it has an *inactivation gate*.

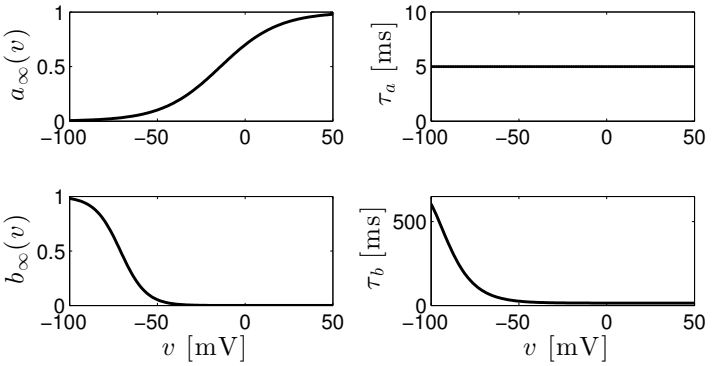

Figure 34.7. *The steady states and time constants of the gating variables in the model A-current of [155].* [A_CURRENT]

The model A-current in [155] is given by

$$I_{\rm A} = \overline{g}_{\rm A}\, ab(-90 - v), \tag{34.1}$$

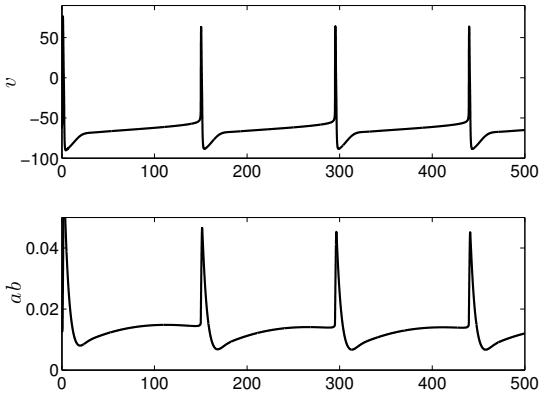

Figure 34.8. *Upper panel: Same as Fig. 34.6, but with A-current defined by eqs. (34.1)–(34.4), with* $\overline{g}_{\mathrm{A}} = 22$ *mS/cm*^{2}*. Lower panel: The product, ab, of the two gating variables of the A-current (see eqs. (34.1)–(34.4)).* [PRE_OLM_WITH_H_AND_A_CURRENTS]

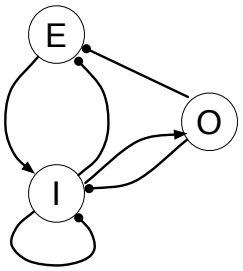

Figure 34.9. *Symbolic depiction of the network of Fig. 34.10. The large circles labeled "E", "I", and "O" represent* populations *of cells. Lines ending in arrows indicate excitation, and lines ending in solid circles indicate inhibition.*

with

$$\frac{dx}{dt} = \frac{x_\infty(v) - x}{\tau_x(v)} \qquad \text{for } x = a, b,$$

$$a_\infty(v) = \frac{1}{1 + \exp(-(v+14)/16.6)}, \quad \tau_a(v) = 5, \tag{34.2}$$

$$b_\infty(v) = \frac{1}{1 + \exp((v+71)/7.3)}, \tag{34.3}$$

$$\tau_b(v) = \frac{1}{\dfrac{0.000009}{\exp((v-26)/28.5)} + \dfrac{0.014}{0.2 + \exp((v+70)/11)}}. \tag{34.4}$$

Note that $a_\infty(v)$ and $b_\infty(v)$ are increasing and decreasing functions of v, respectively. This is why a is called an *activation variable*, and b an *inactivation vari-*

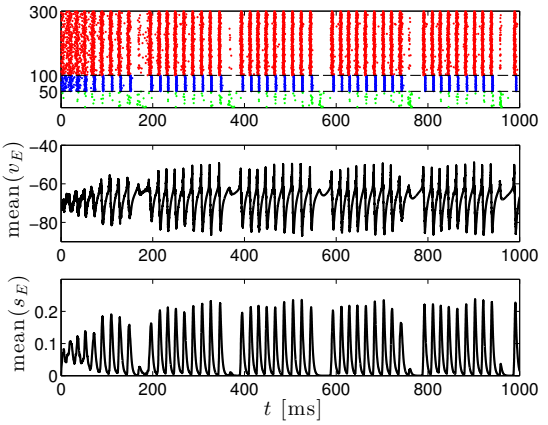

Figure 34.10. *Upper panel: Spike rastergram of a network of 50 O-cells (green), 50 I-cells (blue), and 200 E-cells (red). The parameters are* $\overline{I}_E = 1.8$, $\sigma_E = 0.05$, $\overline{I}_I = 1$, $\sigma_I = 0.1$, $\overline{I}_O = -2$, $\sigma_O = 0.05$, $\hat{g}_{EE} = 0$, $\hat{g}_{EI} = 0.25$, $\hat{g}_{EO} = 0$, $\hat{g}_{IE} = 0.25$, $\hat{g}_{II} = 0.25$, $\hat{g}_{IO} = 0.5$, $\hat{g}_{OE} = 1$, $\hat{g}_{OI} = 0.5$, $\hat{g}_{OO} = 0$, $p_{UV} = 1$ *for all* $U, V \in \{E, I, O\}$ *(all-to-all connectivity). For all synapses, the rise times are 0.5 ms, the times-to-peak are 0.5 ms as well, and the decay times are* $\tau_{d,E} = 3$, $\tau_{d,I} = 9$, *and* $\tau_{d,O} = 20$ *ms. The synaptic reversal potentials are 0 mV for excitatory synapses, and* -75 *mV for all inhibitory synapses. Middle and bottom panels: Means of E-cell voltages and E-cell synaptic gating variables, respectively.* [EIO_1]

able (see Section 3.2). From Fig. 34.7, you see that *inactivation* is fast, but *de-inactivation* is slow: τ_b is small for large v, but large for v below threshold. As a result, the total conductance density $\overline{g}_{\mathrm{A}}ab$ behaves very differently from the total conductance density of an adaptation current: When the neuron fires, $\overline{g}_{\mathrm{A}}ab$ very briefly rises. However, when the membrane potential falls, $\overline{g}_{\mathrm{A}}ab$ rapidly follows it, because a follows v with a short time constant. (In fact, in [134] the activation gate of the A-current was taken to be an instantaneous function of v.) The inactivation gate, which also drops during the action potential, takes some time to recover. This is why there is a prolonged dip in ab following an action potential; see Fig. 34.8. Throughout the remainder of this chapter, we use $\overline{g}_{\mathrm{A}} = 22\,\mathrm{mS/cm^2}$.

The values of ab between two action potentials only varies by about a factor of 2 in Fig. 34.8. So to reasonably good approximation, the A-current adds *tonic inhibition* (namely, inhibition with a constant conductance) to the cell. The question whether the time dependence of ab actually matters to the model of nested gamma-theta oscillations in Section 34.3 will be the subject of exercise 3.

34.3 An E-I-O network generating nested gamma-theta rhythms

Following [155], we add a population of O-cells (model O-LM cells as described in Section 34.2) to a PING network; see Fig. 34.9. In analogy with eqs. (30.1) and (30.2), we take the drive to the k-the O-cell to be

$$I_{O,k} = \overline{I}_O \left(1 + \sigma_O Z_k\right), \tag{34.5}$$

where $\overline{I}_O$ and $\sigma_O \geq 0$ are fixed numbers, and the Z_k are independent standard Gaussians. The resulting network can indeed generate nested gamma-theta oscillations; see Fig. 34.10 for an example. As in previous simulations, each cell of the network was initialized at a random phase with uniform distribution on its limit cycle.

Note that in Fig. 34.10, there are no E-to-O synapses. In [91, Fig. 3], nested gamma-theta oscillations were shown for an E-I-O network with positive, albeit very weak, E-to-O conductance. For more on this issue, see exercise 1.

Exercises

34.1. (∗) In Fig. 34.10, there is no feedback from E-cells to O-cells, as indicated in Fig. 34.9. In [91, Fig. 3], there is such feedback, but it is quite weak. It is known, however, that there are projections from CA1 pyramidal cells to CA1 O-LM cells [148].

(a) What happens if we add E-to-O synapses, say with $\hat{g}_{EO} = 0.1$, in the simulation of Fig. 34.10? Try it out. You will see that the O-cells don't reach near-synchrony now. Some fire on each cycle of the gamma oscillation. As a result, there is no nested gamma-theta rhythm, just an ongoing gamma rhythm slowed down by the O-cells.

(b) Suppose there is some initial mechanism that roughly synchronizes the O-cells, maybe some excitatory signal that makes many of them fire. To model this, suppose that the initial phases of the O-cells are chosen at random not between 0 and 1, but between 0 and 0.1. Is there then a nested gamma-theta rhythm even when $\hat{g}_{EO} = 0.1$?

34.2. (∗) When the I-to-O connections are cut in Fig. 34.10, there is nothing to synchronize the O-cells any more, and the nested gamma-theta rhythm is lost. (Try it!) But now suppose that as in exercise 1b, we approximately synchronize the O-cells at the start of the simulation, by choosing their initial phases randomly between 0 and 0.1, not between 0 and 1. Does this restore the nested gamma-theta oscillations for a significant amount of time?[29]

[29] It couldn't restore them forever: There is nothing to enforce synchrony of the O-cells now, other than the initialization, and because of the heterogeneity of the external drives to the O-cells, their synchrony must disintegrate eventually, and with it the nested gamma-theta oscillation.

34.3. ($*$) In the simulation of Fig. 34.10, replace ab by 0.013, which is approximately its average subthreshold value in Fig. 34.8 (lower panel). This means replacing the A-current by *tonic inhibition* (inhibition with constant conductance). How does the figure change?